Digital pulse deconvolution method for current tails of NaI(Tl) detectors*

Guo-Qiang Zeng(曾国强)[1)] Jian Yang(杨剑)[2)] Ming-Fu Yu(喻明福)
Kai-Qi Zhang(张开琪) Qing Ge(葛青) Liang-Quan Ge(葛良全)
Key Laboratory of Applied Nuclear Techniques in Geosciences Sichuan, Chengdu University of Technology, Chengdu 610059, China

Abstract: To overcome the problem of pulse pile-up at high count rates, a digital deconvolution algorithm is used to remove the exponential current tails of NaI(Tl) detectors, so as to obtain a current unit impulse. Then a narrow pulse can be obtained through pulse shaping. The pulse deconvolution technique can thoroughly eliminate the influences of ballistic deficit and improve traditional pulse shaping systems in both pulse throughput and energy resolution. To demonstrate this method, the energy spectrum of a ^{137}Cs radioactive source was measured. When the shaping time constant is 1.5 μs, traditional pulse shaping systems yielded a 6.99% energy resolution and 68 kcps count rate, while the new pulse deconvolution technique, used to improve traditional pulse shaping systems, yielded a 6.37% energy resolution and 102 kcps count rate.

Keywords: deconvolution, pulse shaping, digital pulse processing, decay time, ballistic deficit

PACS: 29.40.Mc, 29.85.Ca, 84.30.Sk **DOI:** 10.1088/1674-1137/41/1/016102

1 Introduction

The dominant decay time of the scintillation pulses in a NaI(Tl) detector is a prevailing 230 ns component [1]. Due to its slow time response, the problem of pulse pile-up still cannot be resolved effectively for high count rate applications [2]. With the development of high-speed sampling techniques, the directly digitized current signals of NaI(Tl) detectors can be implemented to obtain a narrow pulse [3]. However, this means the detector should be equipped with a high-speed analog-to-digital converter (ADC) and corresponding high-speed signal processing circuits, all of which will increase the cost of the system. However, under the basis of newly developed convolution and deconvolution methods, studies of direct pulse deconvolution have already been performed. This technique can effectively reduce the pulse width by removing the exponential tails of the NaI(Tl) detector. More recently, deconvolution methods for a NaI(Tl) detector and a photomultiplier tube (PMT) have been reported in Ref. [4], where the pulses could be deconvoluted into 200 ns ultra-narrow pulses by using 200 MHz sampling frequency. Apart from this, Ref. [5] studied the deconvolution methods of signal conditioning electronics (CR and RC circuits) by using a silicon drift detector (SDD), where there is no need to deconvolute the detector pulse due to the fast time response of the SDD. In this work, we study the pulse deconvolution technique for a NaI(Tl)-PMT unit based on a traditional low-speed digital signal processing system, where a RC circuit is used to integrate the current signal over time. By means of the RC circuit, the ADC sampling frequency can be reduced to avoid the directly digitized current signals. Besides, the RC circuit can also reduce the signal noise. In this low-cost way, the pulse deconvolution technique can thoroughly eliminate the influence of ballistic deficit and improve both pulse throughput and energy resolution. This paper is divided into five parts. The second part presents the details of pulse processing. In the third part, MATLAB and field programmable gate arrays (FPGA) are applied to verifying this technique. The fourth part is used to show experimental results. The final part gives some conclusions.

2 Pulse processing

2.1 Pulse signal

For NaI(Tl) crystal, the typical decay time of a scintillation pulse includes a fast component and a slow com-

Received 3 September 2016
* Supported by National Natural Science Foundation of China (41474159), Sichuan Youth Science & Technology Foundation (2015JQ0035) and Key Laboratory of Applied Nuclear Techniques in Geosciences Sichuan (gnzds2014006)
1) E-mail: 24829500@qq.com
2) E-mail: 22105653@qq.com

ponent [6], but we only took the slow component, which plays the dominant role, into consideration in this study. The NaI(Tl) crystal is typically coupled to a PMT, and the light pulse is converted into current signal, given by Eq. (1), by the PMT [7]:

$$I(t)=\frac{Q}{\tau_0}\mathrm{e}^{-\frac{t}{\tau_0}}u(t), \tag{1}$$

where $u(t)$ is the unit step signal, τ_0 is the decay time of NaI(Tl) and Q is the total electric charge generated by one current signal. The electric charge is collected by the RC circuit, which can broaden the pulse width and reduce the signal bandwidth. Current signal $I(t)$ is converted into voltage pulse $v(t)$, as shown in Eq. (2), through the RC circuit:

$$v(t)=\frac{QR}{RC-\tau_0}(\mathrm{e}^{-\frac{t}{RC}}-\mathrm{e}^{-\frac{t}{\tau_0}})u(t), \tag{2}$$

where RC is the decay time of the RC circuit. Figure 1 shows the pulse signals $v(t)$ (RC=1000 ns and RC=230 ns) and $I(t)$ (directly digitized current signal). The width of the voltage pulses $v(t)$ increases significantly with the increase of RC, and the rising edges of the voltage pulses $v(t)$ become slower. Hence, the RC circuit can effectively reduce signal bandwidth, which is good for ADC sampling. As long as the sampling frequency is greater than twice the signal bandwidth, to avoid frequency aliasing, we should reduce RC as much as possible to avoid pulse pile-up. Because a 40 MHz ADC was used in this study, the optimal value of RC is 230 ns, and the corresponding pulse signal bandwidth is about 10 MHz.

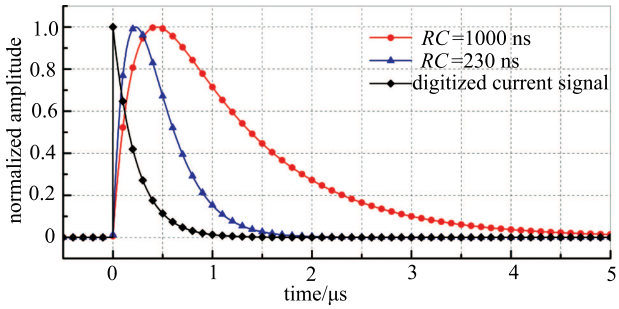

Fig. 1. Current signal and voltage pulse signal.

2.2 Pulse deconvolution

In order to convert the current signal $I(t)$ to a current unit impulse $\delta_{\mathrm{i}}(t)$, we analyze an ideal uni-exponential voltage pulse $s(t)$ and sampled bi-exponential voltage pulse $v(t)$, as shown in Fig. 2, to deduce the functional relation of conversion between them through digital methods.

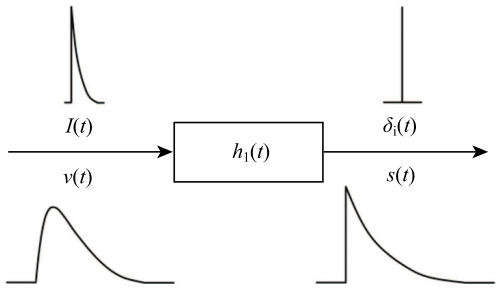

Fig. 2. Transfer function model of deconvolution.

When $\tau_0=0$ in Eq. (2), it is equivalent to a current unit impulse $\delta_{\mathrm{i}}(t)$ charging the RC circuit to obtain an ideal uni-exponential voltage pulse $s(t)$, as given by Eq. (3).

$$s(t)=\frac{Q}{C}\mathrm{e}^{-\frac{t}{RC}}u(t). \tag{3}$$

Then, a Fourier transform is used respectively for $v(t)$ and $s(t)$ to obtain Eq. (4) and Eq. (5).

$$V(\mathrm{j}\omega)=\frac{QR}{RC-\tau_0}\left(\frac{1}{\frac{1}{RC}+\mathrm{j}\omega}-\frac{1}{\frac{1}{\tau_0}+\mathrm{j}\omega}\right), \tag{4}$$

$$S(\mathrm{j}\omega)=\frac{Q}{C}\left(\frac{1}{\frac{1}{RC}+\mathrm{j}\omega}\right). \tag{5}$$

Equation (6) is the frequency response of $v(t)$ being converted into $s(t)$.

$$H_1(\mathrm{j}\omega)=\frac{S(\mathrm{j}\omega)}{V(\mathrm{j}\omega)}=1+\mathrm{j}\omega\tau_0. \tag{6}$$

Then, in order to obtain the transfer function in the time domain, as shown in Eq. (7), a Fourier inverse transform is used on Eq. (6).

$$s(t)=v(t)+\tau_0\frac{\mathrm{d}v(t)}{\mathrm{d}t}. \tag{7}$$

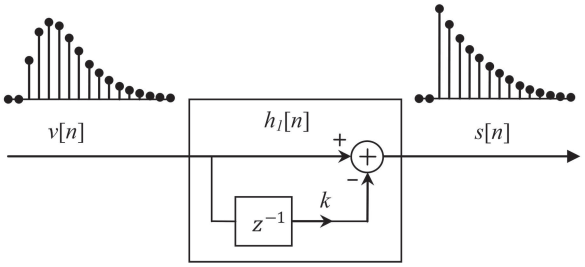

Fig. 3. Recursive method of the bi-exponential pulse being converted into a uni-exponential pulse.

Equation (8) is the discretization of Eq. (7):

$$s[n] = v[n] - k \cdot v[n-1], \tag{8}$$

where $k = \mathrm{e}^{-\frac{T_\mathrm{s}}{\tau_0}}$, and T_s is the ADC sampling period. As shown in Fig. 3, the function of the difference Eq. (8) is equivalent to deconvoluting the original bi-exponential pulse $v[n]$ to a remarkable uni-exponential pulse $s[n]$.

2.3 Pulse shaping

The deconvoluted outputs of the original bi-exponential pulses need to be processed through pulse shaping, which can effectively reduce the electronic noise and increase the signal-to-noise ratio (SNR) [8, 9]. Traditional pulse shaping methods include quasi-Gaussian, triangle, trapezoid, cusp-like, $1/f$ and so on [10–13]. Trapezoids have been extensively applied in pulse shaping by virtue of their excellent energy resolution, so we adopted a trapezoidal shaper. The trapezoidal pulse shaping algorithm uses the form of a recursive difference equation [14], as given in Eqs. (9)–(12), in the time domain, which can output the results in real time and reduce the multiplication operations:

$$\delta[n] = s[n] - d \cdot s[n-1], \tag{9}$$

$$p[n] = \delta[n] - \delta[n-a] - \delta[n-a-b] + \delta[n-2a-b], \tag{10}$$

$$q[n] = q[n-1] + p[n], \tag{11}$$

$$y[n] = y[n-1] + q[n], \tag{12}$$

where $d = \mathrm{e}^{-\frac{T_\mathrm{s}}{RC}}$, a is the hypotenuse width of the trapezoid and b is the flat-top width of the trapezoid. When b =0, it is a triangular shaper. The recursive method of the trapezoidal shaper using difference equations is shown in Fig. 4.

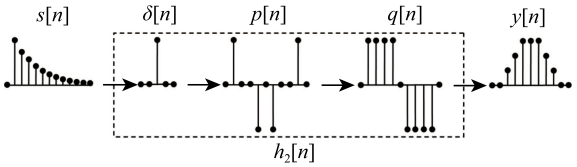

Fig. 4. Recursive method of trapezoidal shaper.

3 Algorithm verification

3.1 Algorithm simulation

Simulink is the simulation environment of MATLAB, and can be rapidly applied to algorithm development and numerical calculation. The original pulse data from a FPGA are loaded into the MATLAB workspace, then a from workspace module is used to import data into Simulink. As shown in Fig. 5(a), by using the pulse deconvolution technique, the original bi-exponential pulses were converted into uni-exponential pulses. Moreover, the amplitude deficit of the original pulse was restored. Figure 5(b) shows the results of triangular pulse shaping. As the triangle has no flat-top to overcome the ballistic deficit, there are lots of serious deformations and tails in the original pulse shaping. By using the pulse deconvolution technique, deconvoluted pulse shaping can thoroughly eliminate the influences of ballistic deficit Fig. 5(c) shows the results of trapezoidal pulse shaping. The trapezoidal flat-tops of the original pulse shaping are already indistinguishable. In addition, the falling edge of the previous pulse shaping overlaps with the rising edge of the subsequent one due to the serious tails, which would result in the amplitude of subsequent pulse shaping being greater than the previous one. But actually the amplitude of the previous one is greater than the subsequent one. Using the pulse deconvolution technique can avoid pulse pile-up to obtain the real amplitude.

3.2 Hardware verification

A low-cost ALTERA EP4CE6 series FPGA and low power dissipation ADI AD9224, 12-Bit and 40 MSPS monolithic ADC were used in this study. Figure 6 is the logic diagram of the pulse shaping algorithm in the FPGA. Digital pulse processing, in the FPGA, consists of three main modules: pulse shaper, pulse deconvolver and external interface. In addition, a parameters module, which is a register array, stores the parameters of the other modules. So the parameters of pulse shaping can be modified conveniently by changing registers.

The parameters of $d = \mathrm{e}^{-\frac{T_\mathrm{s}}{RC}}$ and $k = \mathrm{e}^{-\frac{T_\mathrm{s}}{\tau_0}}$ are float-point type. In order to improve operating speed and reduce data memory, float-point operations in FPGA should be avoided. Both d and k are between 1 and 0. They can be converted into fractions. So it can turn into integer multiplication and integer division respectively operating with numerator and denominator. Besides, in order to avoid the situation where first difference operations and then integral operations would amplify noises that cause baseline shift [15], we use the method of first integral operations and then difference operations for all, so the deconvolution algorithm is placed at the end of pulse shaping.

4 Results and discussion

We applied a NaI(Tl) crystal (size: ϕ76 mm×76 mm) coupled with a PMT (ϕ76 mm CR160-01) from Hamamatsu as the front-end detector to measure a ^{137}Cs 662 keV radioactive source. Figure 7 shows the measured results of energy spectrum for 6, 3 and 1.5 μs shaping time constant respectively. When the traditional shaper system was adopted, there was serious pile-up for the 6 μs shaping time constant, and the count rate was only 12 kcps. As the shaping time constant decreased to

3 μs, the count rate was increased to 39 kcps. With the decrease of the shaping time constant to 1.5 μs, the count rate reached 68 kcps. However, when the pulse deconvolution technique was used to improve traditional pulse shaping for the 1.5 μs shaping time constant, count rates were further elevated, reaching 102 kcps. The higher count rates are basing on the fact that the pulse deconvolution technique improves pile-up discrimination ability and reduces discard of pulse pile-up.

Figure 8 shows the relation of shaping time constant to full width at half maximum (FWHM) of the energy spectra at 662 keV in Fig. 7. It can be seen that for the traditional shaper, the smaller the shaping time constant the poorer the energy resolution. However, the amplitude extraction using the pulse deconvolution technique is more accurate, so its energy resolution is not degraded.

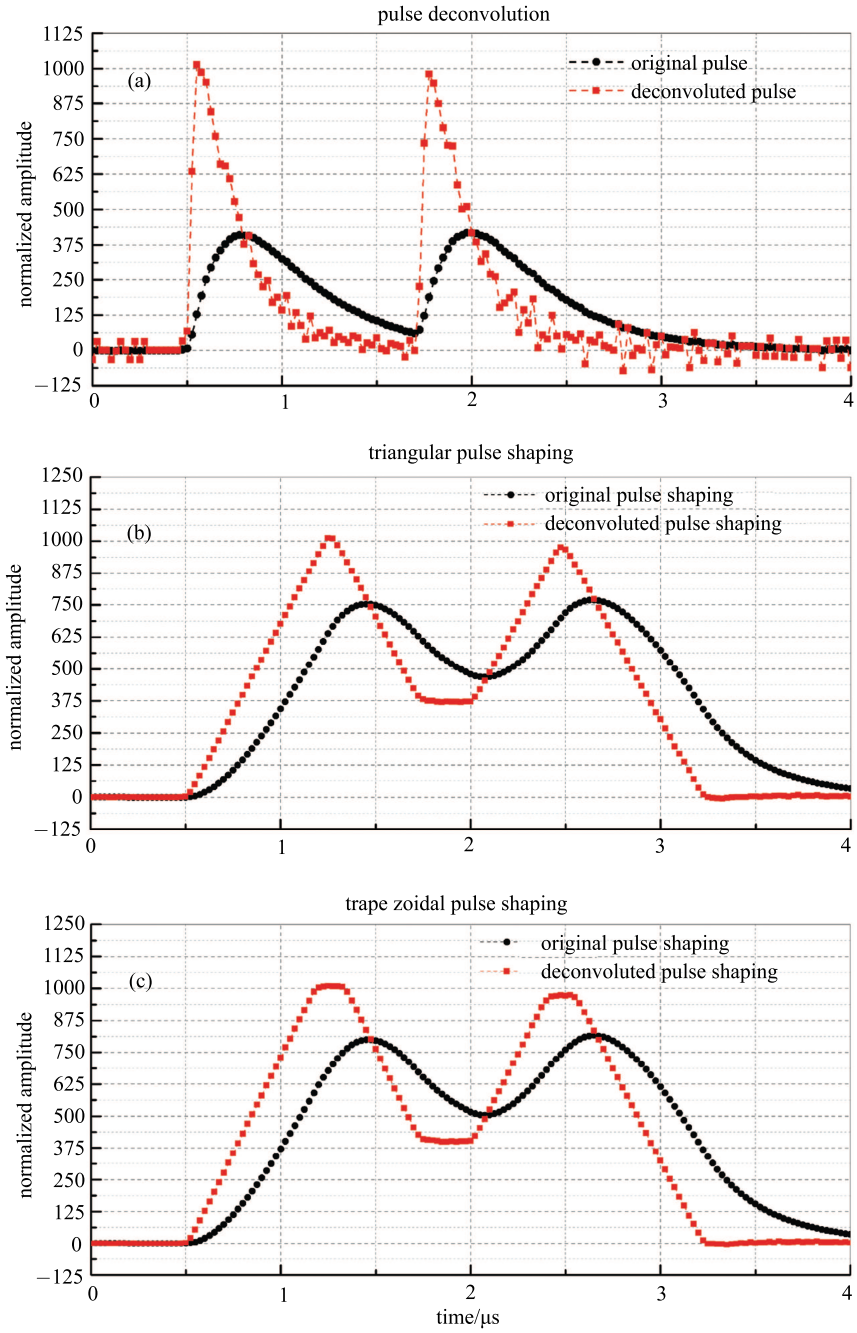

Fig. 5. (a) Original pulses and the deconvoluted pulses; (b) The results of triangular pulse shaping ($a=30$, $b=0$); (c) The results of trapezoidal pulse shaping ($a=27$, $b=6$).

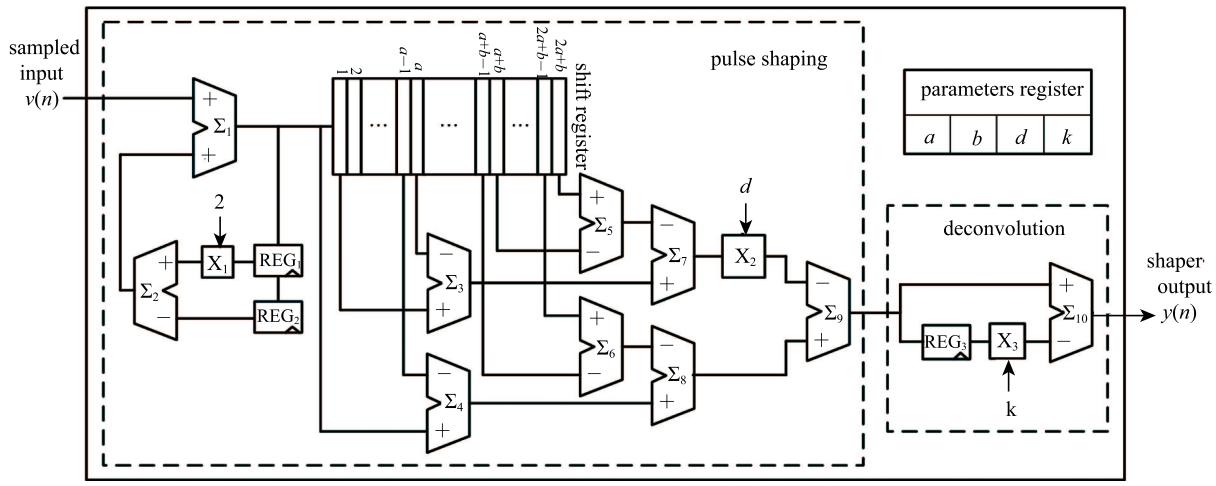

Fig. 6. Logic diagram of algorithm implementation in FPGA.

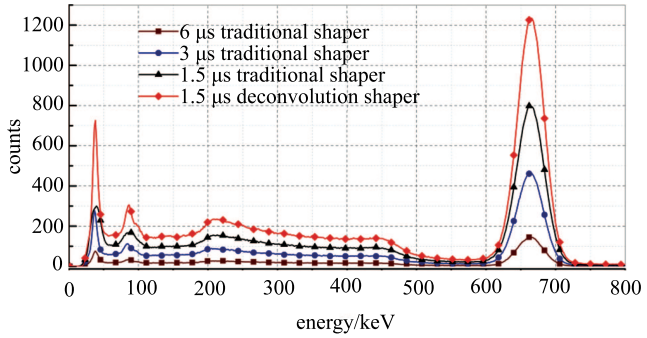

Fig. 7. Measured energy spectrum of ^{137}Cs.

5 Conclusion

For high count rates applications, the shaping time constant should be reduced to improve the pulse throughput. However, NaI(Tl) crystal has a slow scintillation pulse, and traditional pulse shaping has serious tails due to ballistic deficit. This study presents a pulse deconvolution technique by analyzing the digital conversion between the original bi-exponential and ideal uni-exponential pulse. This technique is applied to deconvolute the exponential current signal to the current unit impulse, which can thoroughly eliminate the influence of ballistic deficit. Lastly, the technique was implemented in a hardware system. By improving the traditional pulse shaping, the pulse deconvolution technique not only improves the energy resolution from 6.99% to 6.37%, but also increases the pulse throughout from 68 kcps to 102 kcps. So this technique can obtain both high pulse throughput and excellent energy resolution.

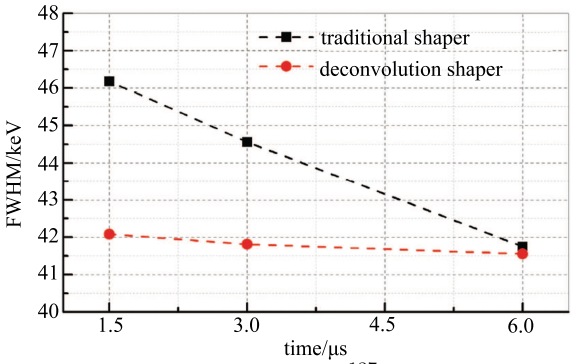

Fig. 8. Measured FWHM of ^{137}Cs with different trapezoidal widths.

References

1 R. Hofstadter, Phys. Rev., **72**(11): 1120–1121 (1947)
2 C. Imperiale, A. Imperiale, Measurement, **30**(1): 49–73 (2001)
3 A. D. Fulvio, T. H. Shin, M. C. Hamel et al, Nucl. Instrum. Methods Phys. Res. A, **806** :169–174 (2016)
4 W. Xiao, A. T. Farsoni, H. Yang et al, Nucl. Instrum. Methods Phys. Res. A, **769**: 5–8 (2015)
5 V. T. Jordanov, Nucl. Instrum. Methods Phys. Res. A, **805**: 63–71 (2016)
6 W. S. Choong, G. Bizarri, N. J. Cherepy et al, Nucl. Instrum. Methods Phys. Res. A, **646**: 95–99 (2011)
7 W. Xiao, A. T. Farsoni, H. Yang et al, Nucl. Instrum. Methods Phys. Res. A, **763**: 170–173 (2014)
8 E. Gatti, A. Geraci, G. Ripamonti, Nucl. Instrum. Methods Phys. Res. A, **381**: 117–127 (1996)
9 A. Regadio, J. Tabero, S. Sanchez-Prieto, Nucl. Instrum. Methods Phys. Res. A, **811**: 25–29 (2016)
10 H. Q. Zhang, L. Q. Ge, B. Tang et al, Nucl. Sci. Tech., **24**(6): 112–117 (2013)
11 V. T. Jordanov, G. F. Knoll, Nucl. Instrum. Methods Phys. Res. A, **345**: 337–345 (1994)
12 A. I. Kalinin, V. A. Bednyakov, Nucl. Instrum. Methods Phys. Res. A, **538**: 718–722 (2005)
13 V. T. Jordanov, Nucl. Instrum. Methods Phys. Res. A, **505**: 347–351 (2003)
14 J. Lanchares, O. Garnica, J. L. Risco-Martin et al, Nucl. Instrum. Methods Phys. Res. A, **727**: 73–83 (2013)
15 M. Kafaee, A. Moussavi-Zarandi, J. Korean Phys. Soc., **68**(8): 960–964 (2016)